Appl. Phys. B 81, 921–926 (2005)
DOI: 10.1007/s00340-005-2017-9

Applied Physics B
Lasers and Optics

P.L. RAMAZZA[1,✉]
U. BORTOLOZZO[2]
S. BOCCALETTI[1]
F.T. ARECCHI[3]

Localized structures in an optical feedback interferometer: properties and interactions

[1] Istituto Sistemi Complessi CNR, Firenze, Italy
[2] Institute Non Lineaire de Nice, France
[3] Universita' di Firenze, Italy

Received: 13 May 2005/Accepted: 8 September 2005
Published online: 28 October 2005 • © Springer-Verlag 2005

ABSTRACT The occurrence of localized structures in a nonlinear optical experiment is a robust phenomenon, persisting in a wide region of the parameter space. We demonstrate how different control parameters determine several properties of localized structures; among these of particular relevance are the contrast and the amplitude and frequency of the oscillations appearing on the tails of the structures. Tuning these oscillations modifies the interactions between pairs of localized structures, thus resulting in a substantial modification of their bound-state spectrum.

PACS 42.65.Tg; 05.45.Yv; 42.65.Sf

1 Introduction

Experimental observations of localized structures (LS) have been offered in different fields, such as fluid dynamics [1], chemistry [2], granular materials [3] and nonlinear optics [4–10]. In this last framework, optical localized structures have been observed in photorefractive cavities [4, 5], in passive nonlinear feedback interferometers [6–8] and in microresonators filled with semiconductor media [9, 10].

In the context of optics, a difference is sometimes stressed between 'localized structures' and 'cavity solitons', the latter being localized structures occurring in a system comprising a resonant optical cavity. Following this distinction, in this paper we refer to our solitary structures always as localized structures (LS), since there is no cavity in our experiment. Apart from this aspect, the LS here investigated are of the same nature as the cavity solitons reported by other groups [7, 10]; by this we mean that, in all cases, LS arise from a homoclinic connection of the lower uniform branch, passing close to an upper patterned branch.

In this paper we review the properties of LS in a nonlinear optical interferometer, formed by a liquid crystal light valve with optical feedback. In Sect. 2 we study the range of existence of the LS in parameter space. In Sect. 3 we discuss the modifications of these structures observed in response to the variation of several external control parameters. These parameters provide a sensitive tool to control the most important features of the localized structures, including their stability, shape and interaction properties. Section 4 is devoted to the study of the effect of a specific parameter variation on the interactions between pairs of LS.

✉ Fax: +39 055 233 77 55, E-mail: pier@ino.it

2 Localized structures in the liquid crystal light valve with feedback

Our experimental setup is a liquid crystal light valve (LCLV) inserted in an optical feedback loop, in which both diffractive and interferential effects are present. The system is shown in Fig. 1. The LCLV is formed by a nematic liquid crystal (LC) cell, followed by a mirror and a layer of photoconductive material [11]. A voltage of rms amplitude V_0 and frequency ν is applied to the series of these three elements. When the LCLV is inserted into an optical feedback loop, the fraction V_{LC} of voltage that falls across the LC cell is determined by both V_0 and the light intensity I_{fb} fed back to the photoconductive layer. Under the effect of V_{LC}, the LC reorients, thus inducing a space-dependent phase retardation on a homogeneous input beam injected into the optical system. For a broad parameter range, the phase retardation can be considered proportional to I_{fb}. In the jargon of nonlinear optics,

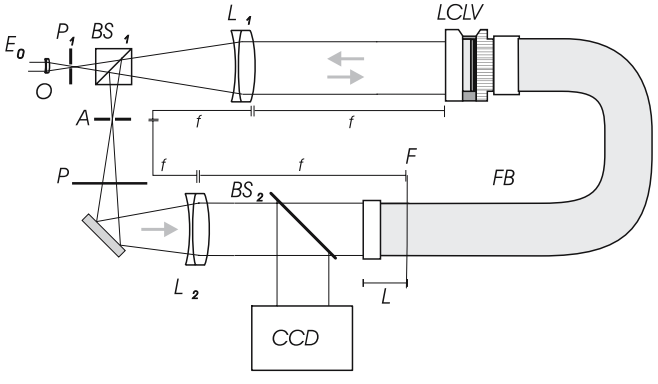

FIGURE 1 Experimental setup. $E_0 =$ input field; $O =$ microscope objective; $P_1 =$ pinhole; $A =$ iris; BS_1, $BS_2 =$ beam splitters; LCLV $=$ liquid crystal light valve; L_1, $L_2 =$ lenses of focal length f; $P =$ polarizer; $FB =$ fiber bundle; CCD $=$ video camera; $F =$ image plane of the LCLV. The overall free propagation of a negative distance L results in a change of the system nonlinearity from self-defocusing, as it would be for the LCLV alone, to self-focusing. In the experiments here reported, $L = 25$ cm (from Ref. [16])

this amounts to saying that, in the closed-loop configuration, the LCLV operates as a Kerr-like medium.

Pattern-forming instabilities have been studied in this system using several feedback configurations [12–14], in order to identify the role of different physical mechanisms (diffraction, diffusion, nonlocal interactions, etc.) in determining the observed selection of patterns. Here we concentrate on an experimental setup that includes both diffraction and interference in the feedback path.

Indeed, diffraction is controlled by lenses L_1 and L_2 inserted within the system, and by the position of the plane F corresponding to the input of the fiber bundle; interference between the components of the light polarized parallel and perpendicular to the optical axis of the liquid crystals is obtained by means of their projections onto the transmissive axis of the polarizer P. Under these conditions, the equation governing the space–time evolution of the phase $\varphi(\boldsymbol{r}, t)$ induced by the LC on the input beam is [15, 16]

$$\tau \frac{\partial \varphi(\boldsymbol{r}, t)}{\partial t} = -(\varphi(\boldsymbol{r}, t) - \varphi_0) + l_\mathrm{d}^2 \nabla_\perp^2 \varphi(\boldsymbol{r}, t) + \alpha I_\mathrm{fb} \,. \tag{1}$$

Here, $\varphi_0 \equiv \varphi_0(V_0, \nu)$ is the space- and time-independent phase retardation induced by the LCLV in the absence of feedback intensity, l_d is the diffusion length of the liquid crystals and α gives the sign and strength of the Kerr nonlinearity. Furthermore, the feedback intensity I_fb is given by

$$I_\mathrm{fb} = I_0 \left| \exp(-\mathrm{i} L \nabla^2 / 2k_0) \left(B \, \mathrm{e}^{-\mathrm{i}\varphi} + C \right) \right|^2 . \tag{2}$$

The diffraction operator $\exp(-\mathrm{i} L \nabla^2 / 2k_0)$ expresses in a formal way the fact that transverse Fourier components of the electric field at frequency q undergo, by free propagation, a phase retardation $\mathrm{i} L q^2 / 2k_0$ with respect to the on-axis field.

In (2), $I_0 = |E_0|^2$ represents the linearly polarized input beam intensity, L is the free propagation length along the optical path, $k_0 = 2\pi/\lambda$ is the optical wavenumber and the parameters B and C are given by

$$B = \cos\theta_1 \cos\theta_2 \,, \qquad C = \sin\theta_1 \sin\theta_2 \,, \tag{3}$$

θ_1 and θ_2 being respectively the angles formed by the input light polarization direction and by the polarizer's P transmissive axis with the LC optical axis. The feedback intensity arises therefore by the interferential sum of the field amplitudes polarized along the LC director, having amplitude B, and perpendicular to it, having amplitude C. In this respect, the device can be considered as a polarization interferometer.

In the following we restrict ourselves to the case $\theta_1 = \theta_2 \equiv \theta$, so that $B = \cos^2\theta$, $C = \sin^2\theta$.

It is evident from (1) that the system has several control parameters; here we focus our attention on $(\theta, I_0, V_0, q_\mathrm{b})$, where θ, I_0 and V_0 have been previously defined and q_b is the spatial frequency bandwidth, controlled by means of an iris A in the Fourier plane. We express q_b in units of the diffractive wavenumber $q_\mathrm{diff} = \sqrt{\pi k_0 / L}$, which is the scale at which the system would patternize in the case of purely diffractive feedback, in the absence of diffusion.

We investigate the range of existence of localized structures. The necessary condition of coexistence of a lower uniform branch and an upper patterned branch is satisfied for a broad range of parameters.

First we notice that, at any value of the triplet $(\theta, I_0, q_\mathrm{b})$, localization of patterns exists for a rather limited range of V_0, corresponding to φ_0 close to π. Only in this situation, indeed, is the required bistability between a low-intensity uniform state and a high-intensity patterned one realized. When φ_0 differs from π by an amount larger than $\simeq 15\%$, the lower branch loses its stability with a supercritical bifurcation leading to other kinds of patterns, so that one of the conditions for localization of structures, namely bistability, is no longer met.

For all the measurements reported in this section, φ_0 has been held fixed at 1.09π. In these conditions, $(q_\mathrm{b}, \theta, I_0)$ are scanned as described below. Initially (q_b, θ) are kept fixed and the system is on the high-intensity patterned branch. At this point I_0 is decreased, leading to the formation of LS, which at smaller intensities die out, leaving the system in the lower homogeneous state. It is to be stressed that the inverse procedure, consisting in an increase of I_0 starting from the homogeneous value, leads to the emergence of delocalized patterns via a subcritical bifurcation. Hence, as is natural in the pres-

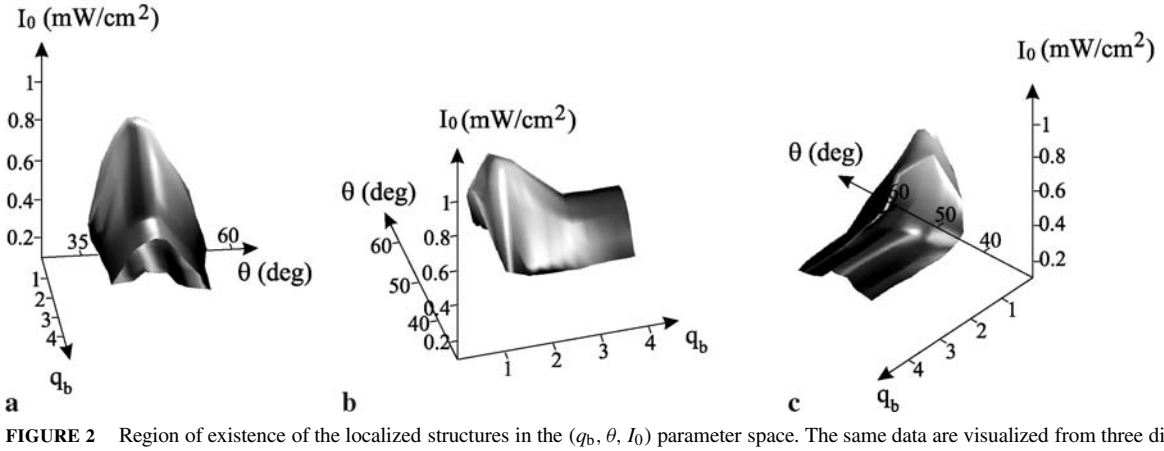

FIGURE 2 Region of existence of the localized structures in the $(q_\mathrm{b}, \theta, I_0)$ parameter space. The same data are visualized from three different perspectives. The value of φ_0 is kept fixed at $1.09\,\pi$. All the data have been obtained by starting the observation at high values of intensity, and then gradually decreasing it (from Ref. [16])

ence of the present scenario, the occurrence of localization depends on the system parameter history.

By scanning (q_b, θ) and repeating the above procedure, we map the volume of existence of the LS displayed in Fig. 2. It is seen here that the formation of LS is not limited to a few particular values of the parameters, but it is observed over broad ranges of (q_b, θ, I_0) as a robust phenomenon.

3 Control of the localized structure properties

The different parameters introduced in Sect. 2 have an important influence in determining not only the existence range of the LS, but also their spatial shape. As a consequence, it is possible to broadly tune the properties of the structures acting on one or more of these variables. Figure 3 shows the dependence of the LS profile upon the intensity I_0, keeping fixed the other parameters (see figure caption for their values). It is apparent that the main effect of increasing I_0 is a corresponding increase of the amplitude of the oscillations on the LS tails. This is due to the fact that the region of the tails is at low intensity, i.e. in a linear unsaturated regime, so that an increase of the pump induces a corresponding considerable increase of the tails' amplitude.

Aside from this, a slight monotonic variation of both the lower and the upper intensity levels is observed. This latter is not visible in the figures presented, since they are saturated in order to visualize the low-intensity details.

In Sect. 4 we will discuss how the modifications of the tails make it possible to tune the LS interactions.

Following the definitions of B and C in (3), we see that a variation of the angle θ affects the values of both the interferential and the diffractive contributions to the feedback intensity. Since these phenomena are responsible for the selection and stability of the two branches involved in the LS formation, it is expected that variations of θ greatly affect the features of the observed LS.

Figure 4 shows how the shape of the structures modifies as θ varies across the range in which localization is observed. Two main effects of the variation of θ appear here. On one hand, due to the tuning of the interferential contribution, the intensities of the lower and upper branches are strongly dependent on θ. Thus, bright localized structures on a very dark

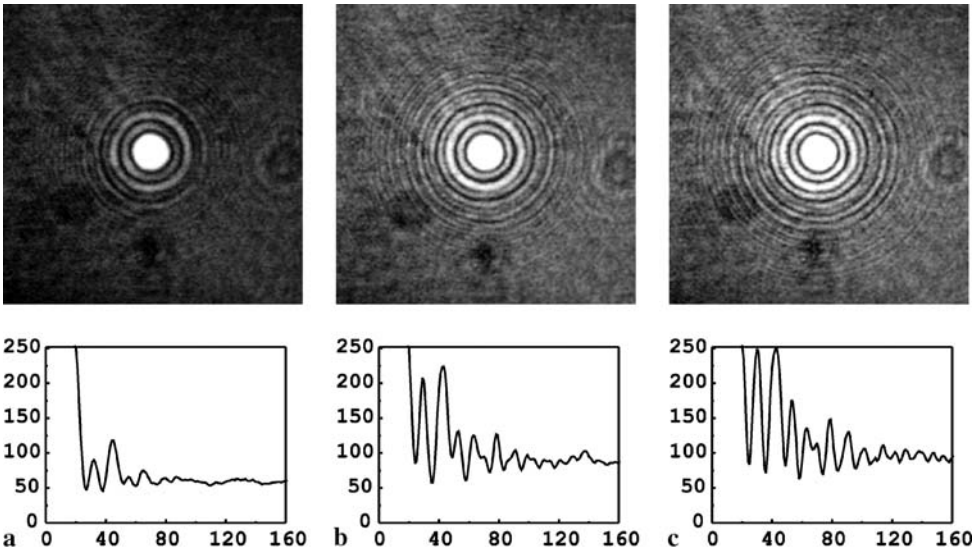

FIGURE 3 Pictures and radial profiles (averaged on the azimuthal coordinate) of the localized structures, for increasing intensity. $I_0 = 360\,\mu W/cm^2$ (**a**); $I_0 = 530\,\mu W/cm^2$ (**b**); $I_0 = 620\,\mu W/cm^2$ (**c**). The other parameters are fixed at $\theta = 45°$, $q_b = 4$, $\varphi_0 = 1.09\pi$ (from Ref. [16])

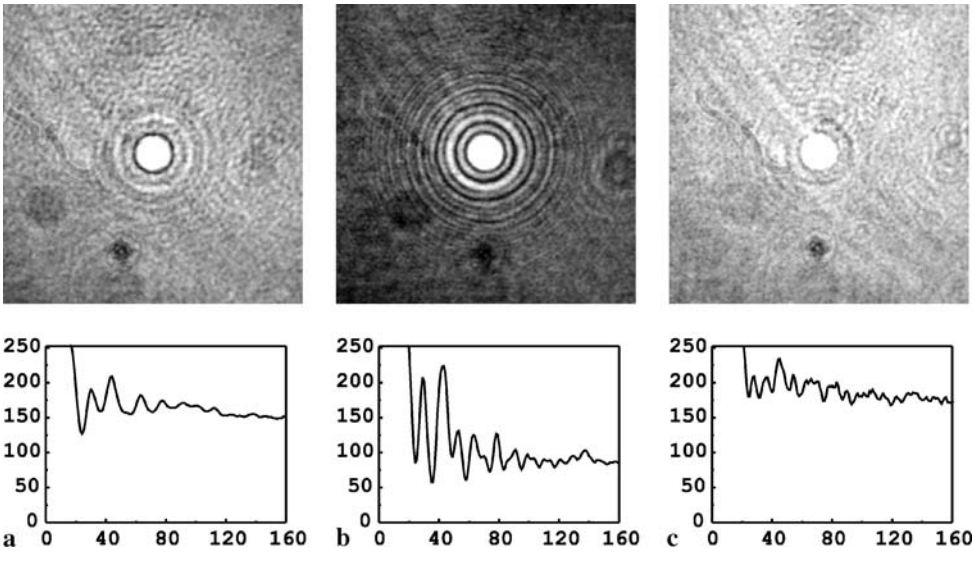

FIGURE 4 Pictures and radial profiles of the localized structures for increasing angle θ. $\theta = 38°$ (**a**); $\theta = 45°$ (**b**); $\theta = 54°$ (**c**). The input intensity is set to a value lying approximately at the center of the existence range of LS for any value of θ (from Ref. [16])

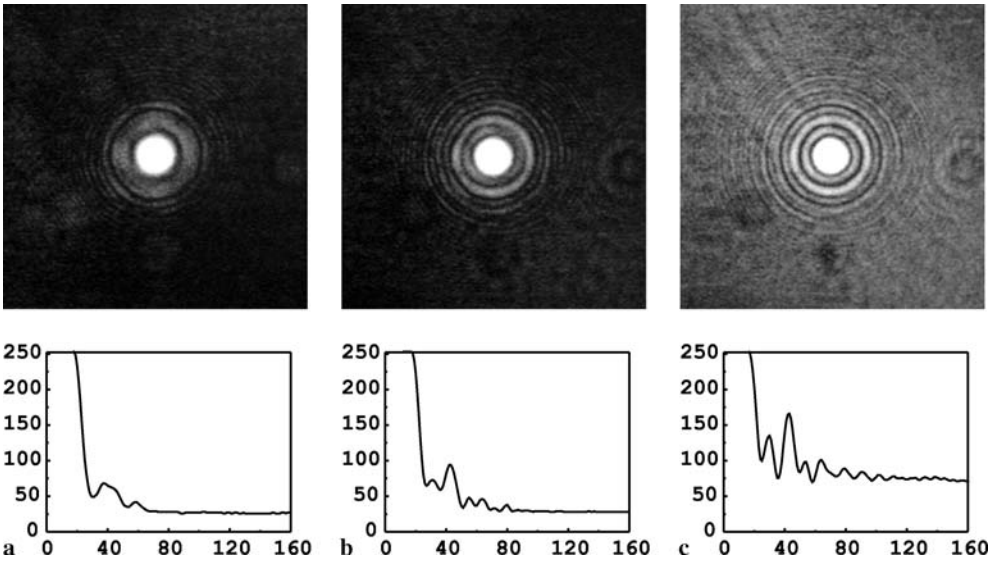

FIGURE 5 Pictures and radial profiles of the localized structures for increasing angle φ_0. $\varphi_0 = \pi$ (**a**); $\varphi_0 = 1.03\pi$ (**b**); $\varphi_0 = 1.07\pi$ (**c**). The other parameters are fixed at $\theta = 45°$, $I_0 = 580\,\mu\mathrm{W/cm^2}$, $q_\mathrm{b} = 4$ (from Ref. [16])

background are observed at $\theta \simeq 45°$, while the intensity difference between the involved branches decreases noticeably at the extrema of the range of localization ($\theta \simeq 38°, \theta \simeq 54°$). On the other hand, the amplitude of the oscillations on the tails is also affected by the value of θ, displaying a clear maximum at $\theta = 45°$.

Let us finally consider the effect on LS of the phase angle φ_0, experimentally controlled via the external voltage applied to the LCLV. Figure 5 reports the LS observed for increasing values of φ_0, starting from $\varphi_0 = \pi$. A first, very clear effect is the modification of the contrast between dark and bright states involved in the formation of the structures. As expected from a qualitative analysis of (3)–(5), the maximum contrast is obtained for $\varphi_0 = \pi$, at any value of θ. Tuning the LS contrast using this parameter can be of interest in view of applications in which these localized structures are used as pixels for the storage and/or the processing of optical information [17, 18].

Besides this effect on contrast, the variation of φ_0 also influences the amplitude and wavelength of the LS tails. This is not surprising, since it is clear from an inspection of the system equations that φ_0 affects the selection of the spatial scales existing in the LS, and in particular on their tails.

4 Localized structure interactions

It has been recognized [7, 19] that the oscillations on the tails are responsible for the interactions between LS, leading eventually to the formation of bound states of the kind shown in Fig. 2. In particular, it has been predicted that the force between a pair of LS is of oscillatory sign as a function of their mutual distance, with a periodicity given by the wavelength of the oscillations on each LS tail. It is also expected that the strength of these forces is proportional to the amplitude of these oscillations.

In this section we investigate how the forces between LS depend on the tail features, using q_b as a control parameter [20]. The modification in the shape of a single LS vs. q_b is shown in Fig. 6. It is seen here that the central peak is rather insensitive to the variations of q_b. The length scale of the oscillations on the tails is instead strongly dependent on

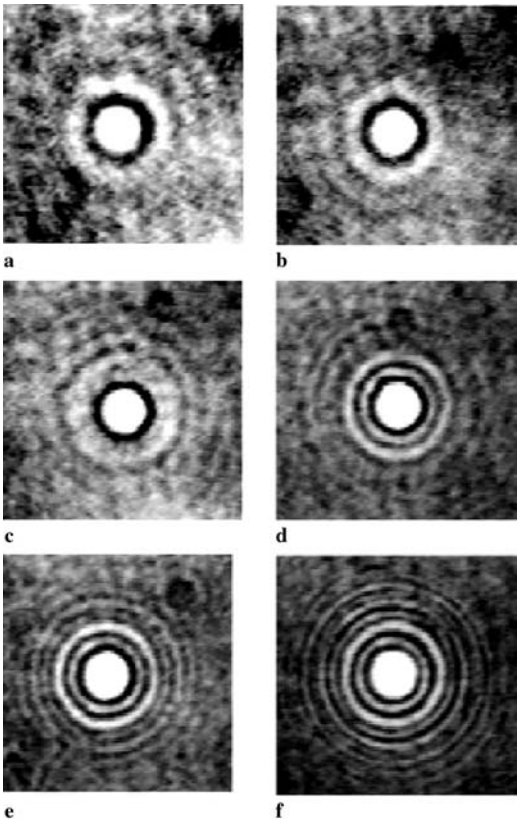

FIGURE 6 Variation of the LS's shape with the system bandwidth, for $\theta = 42°$. Snapshots of the observed LS for (**a**) $q_\mathrm{b} = 1.0$, $I_0 = 700\,\mu\mathrm{W/cm^2}$, (**b**) $q_\mathrm{b} = 1.2$, $I_0 = 620\,\mu\mathrm{W/cm^2}$, (**c**) $q_\mathrm{b} = 1.6$, $I_0 = 520\,\mu\mathrm{W/cm^2}$, (**d**) $q_\mathrm{b} = 2.2$, $I_0 = 480\,\mu\mathrm{W/cm^2}$, (**e**) $q_\mathrm{b} = 2.8$, $I_0 = 460\,\mu\mathrm{W/cm^2}$, (**f**) $q_\mathrm{b} = 4.0$, $I_0 = 460\,\mu\mathrm{W/cm^2}$. The pictures are overexposed at the location of the central peak, in order to allow visualization of low-intensity features on the LS tails. The slight increase of I_0 from the highest to the lowest q_b is suggested by convenience, as may be seen from the skewed profile of the LS domain of existence in the plane (q_b, I_0) (Fig. 2b) (from Ref. [18])

q_b. Namely, this scale decreases for increasing q_b until $q_\mathrm{b} \simeq 3$, and then saturates to a constant value.

The set of our observations indicates that LS have a 'natural' unperturbed shape like that displayed for $q_\mathrm{b} \geq 3$. By con-

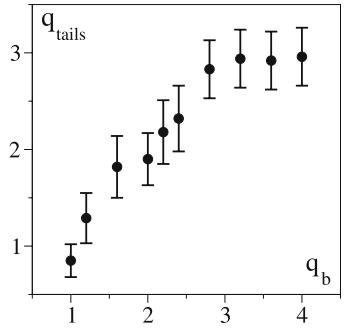

FIGURE 7 Variation in the main frequency of the LS tail oscillations as a function of the system bandwidth. Both q_{tails} and q_{b} are adimensional quantities (see text for definitions) (from Ref. [18])

straining the system to a bandwidth smaller than this value, one is then able to tune the LS profile, imposing oscillations on the tails at a frequency different from the natural one.

The observed LS closely resemble those reported in Ref. [19], in which a subcritical real Swift–Hohenberg equation is studied analytically and numerically.

Using the Swift–Hohenberg model, it is found analytically that the LS tails are described by single spatial scale oscillations, embedded in an exponential envelope that departs from the lower uniform state.

Though the LS tails in our case display some deviations from the above ideal behavior, the qualitative agreement between our observations and the results of the general theory reported in Ref. [19] is satisfactory. In particular, it is possible to identify for each value of q_{b} a dominating spatial scale in the oscillatory tails.

For this purpose, we measure the distance between successive maxima of a single LS and average this quantity over all observed maxima. In this way, we obtain the dominant spatial frequency of the tail oscillations, which is then normalized to q_{diff} and reported as q_{tails} in Fig. 7. The error bars correspond to the measured frequency fluctuations from q_{tails}, reflecting the fact that the tail oscillations are not rigorously at a single spatial scale. Looking at Fig. 7, one easily realizes that q_{tails} practically coincides with q_{b} for $q_{\text{b}} \leq 3$. At higher values of q_{b}, no variations in q_{tails} as well as in the overall LS's profile are observed.

The shape of the tails is responsible for the interactions between localized structures. Namely, while for monotonically decreasing tails one would expect only attractive or repulsive forces between LS, oscillatory tails induce oscillatory signs of the interactions, thus producing both attractive and repulsive forces, depending on the distance between the centers of a pair of LS's [19, 21].

The existence of a discrete set of LS bound states, occurring in the presence of oscillations on the LS tails, has been demonstrated in an optical experiment similar to ours [7].

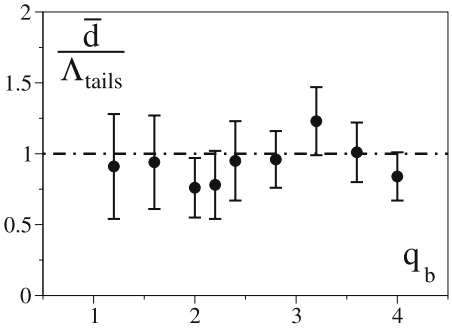

FIGURE 9 $\bar{d}/\Lambda_{\text{tails}}$ vs. q_{b} (see text for definitions). Both quantities are adimensional. Notice that, for all measurements, a constant value of $\bar{d}/\Lambda_{\text{tails}} \sim 1$ is realized within the experimental errors (from Ref. [18])

In Fig. 8 we display a set of different bound states observed for $q_{\text{b}} = 3.6$. We notice that the states form a set that can be ordered following a precise rule, given by simply counting the number of maxima and minima that occur along the segment connecting the two LS centers. We will call this number n the bound state order number. Such a feature is encountered for all values of q_{b}. At small system bandwidths, however, we observe only the first two or three bound states, instead of the entire set shown in Fig. 4. This is probably due to the fact that the binding energy of each state varies with q_{b}, and in some cases it is not sufficient to keep the LS pair tightly bound in the presence of unavoidable system inhomogeneities and fluctuations.

The theory of weak interactions between LS discussed in Ref. [19] predicts that a countable set of bound states exists for a pair of LS. Calling R_n the separation between the centers of the two LS in the nth bound state, it is also predicted that the difference $R_{n+1} - R_n$ is approximately equal to one wavelength of the oscillations appearing on the LS tails.

With reference to our experiment, it follows that tuning of the equilibrium distances should be possible by varying the scale of the oscillations on the tails of each single LS. In order to check this point, we measured the quantities $\Delta_{n,n+1} = R_{n+1} - R_n$, and then averaged them over the bound state order number n. The resulting quantity $\bar{d}$ (normalized to the length Λ_{tails}) is reported vs. q_{b} in Fig. 9. A constant value of the ratio $\bar{d}/\Lambda_{\text{tails}} \simeq 1$ is observed within the errors, indicating that the above-discussed relation between the oscillations on the tails of each LS and the selection rule of bound states is verified. This marks the fact that tuning of the equilibrium distances between LS's in bound states can be quantitatively performed in our experiment.

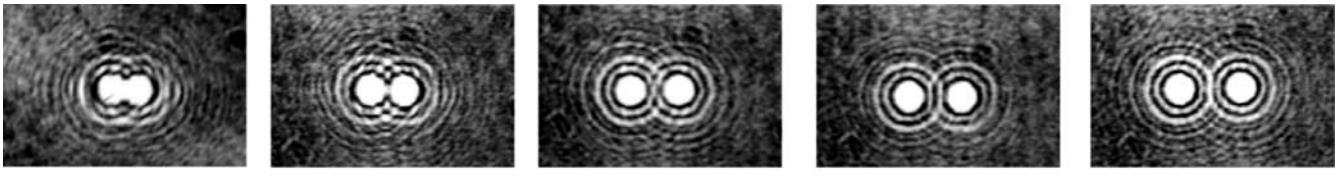

FIGURE 8 Snapshots of different bound states observed at $\theta = 42°$, $q_{\text{b}} = 3.6$, $I_0 = 500\,\mu\text{W/cm}^2$. All patterns (**a**)–(**e**) are obtained by inducing a pair of LS with an increasing initial distance between centers, and letting the system evolve up to the time at which the stationary bound state is realized (from Ref. [18])

REFERENCES

1 E. Moses, J. Fineberg, V. Steinberg, Phys. Rev. A **35**, 2757 (1987)
2 H.H. Rotermund, S. Jakubith, A. von Oertzen, G. Ertl, Phys. Rev. Lett. **66**, 3083 (1991)
3 P. Umbanhowar, F. Melo, H. Swinney, Nature **382**, 793 (1996)
4 M. Saffman, D. Montgomery, D.Z. Anderson, Opt. Lett. **19**, 518 (1994)
5 V.B. Taranenko, K. Staliunas, C.O. Weiss, Phys. Rev. Lett. **81**, 2236 (1998)
6 A. Schreiber, B. Thuring, M. Kreuzer, T. Tschudi, Opt. Commun. **136**, 415 (1997)
7 B. Schapers, M. Feldmann, T. Ackemann, W. Lange, Phys. Rev. Lett. **85**, 748 (2000)
8 P.L. Ramazza, S. Ducci, S. Boccaletti, F.T. Arecchi, J. Opt. B: Quantum S. O. **2**, 399 (2000)
9 V.B. Taranenko, I. Ganne, R.J. Kuszelewicz, C.O. Weiss, Phys. Rev. A **61**, 063 818 (2000)
10 S. Barland, J.R. Tredicce, M. Brambilla, L.A. Lugiato, S. Balle, M. Giudici, T. Maggipinto, L. Spinelli, G. Tissoni, T. Knoedl, M. Miller, R. Jaeger, Nature **419**, 699 (2002)
11 M.A. Vorontsov, M.E. Kirakosyan, A.V. Larichev, Sov. J. Quantum Electron. **21**, 105 (1991)
12 S.A. Akhmanov, M.A. Vorontsov, V.Y. Ivanov, A.V. Larichev, N.I. Zheleznykh, J. Opt. Soc. Am. B **9**, 78 (1992)
13 F.T. Arecchi, S. Boccaletti, S. Ducci, E. Pampaloni, P.L. Ramazza, S. Residori, J. Nonlinear Opt. Phys. Mater. **9**, 183 (2000) and references therein
14 E. Yao, F. Papoff, G.L. Oppo, Phys. Rev. E **59**, 2918 (1999)
15 R. Neubecker, G.L. Oppo, B. Thuering, T. Tschudi, Phys. Rev. A **52**, 791 (1995)
16 P.L. Ramazza, S. Boccaletti, U. Bortolozzo, F.T. Arecchi, Chaos **13**, 335 (2003)
17 Z. Chen, K. McCarthy, Opt. Lett. **27**, 2019 (2002)
18 J. Petter, J. Schroeder, D. Traeger, C. Denz, Opt. Lett. **28**, 438 (2003)
19 I.S. Aranson, K.A. Gorshkov, A.S. Lomov, M.I. Rabinovich, Physica D **43**, 435 (1990)
20 P.L. Ramazza, S. Boccaletti, U. Bortolozzo, S. Ducci, E. Benkler, F.T. Arecchi, Phys. Rev. E **65**, 066204 (2002)
21 C. Schenk, P. Schultz, M. Bode, H.G. Purwins, Phys. Rev. E **57**, 6480 (1998)